Scripta Materialia 173 (2019) 32–36

Contents lists available at ScienceDirect

Scripta Materialia

journal homepage: www.elsevier.com/locate/scriptamat

# Phase transformation induced plasticity in high-strength hexagonal close packed Co with stacking faults

Ruizhe Su [a], Dajla Neffati [b], Jaehun Cho [a], Qiang Li [a], Jie Ding [a], Haiyan Wang [a], Yashashree Kulkarni [b,*], Xinghang Zhang [a,*]

[a] School of Materials Engineering, Purdue University, West Lafayette, IN 47907, USA
[b] Department of Mechanical Engineering, University of Houston, Houston, TX 77204, USA

ARTICLE INFO

*Article history:*
Received 22 April 2019
Received in revised form 9 July 2019
Accepted 20 July 2019
Available online xxxx

*Keywords:*
Cobalt
Stacking faults
Pillar compression
Phase transformation
Molecular dynamics simulation

ABSTRACT

Deformation twinning and dislocation glide are two primary deformation mechanisms in hexagonal close packed (HCP) metals. Here we show, *via in situ* micropillar compression tests, that HCP Co pillars with high-density stacking faults exhibit a high yield strength and significant plasticity. Transmission electron microscopy studies reveal the formation of extensive face-centered cubic (FCC) Co phase after deformation. Molecular dynamics simulations confirm the deformation induced phase transformation, and shed light on the deformation mechanisms in HCP Co with pre-existing stacking faults. This study provides new insights into achieving high strength and plasticity in HCP metals *via* stacking faults and phase transformation.



Cobalt (Co) and its alloys have various applications in high-strength structural materials, magnetic devices as well as corrosion and wear resistant coatings [1–5]. At room temperature, Co has stable hexagonal close-packed (HCP) structure and a small fraction of metastable face centered cubic (FCC) structure due to the low stacking fault energy (SFE) of HCP Co, 31 mJ/m$^2$ [6]. Planar defects such as twin boundaries (TBs) and stacking faults (SFs) have been extensively studied in FCC metals [7–35]. It has been shown that TBs and SFs can strengthen FCC metals by blocking the transmission of dislocations. Meanwhile, there are numerous studies that show partial dislocation-planar defect interactions and detwinning could also provide mobile dislocations and thus improve the ductility [18,30,36–41]. However, there are few studies on deformation mechanisms of HCP metals with preexisting SFs. It has been reported that high density SFs in Mg alloy can increase yield strength by impeding the movement of dislocations [42].

HCP metals are generally less ductile than FCC metals due to insufficient number of independent slip systems, which does not satisfy the von Mises criterion [43,44]. Another deformation mechanism for HCP metals - deformation twinning - can also accommodate plastic deformation and contribute to tensile ductility [45–49]. However, when grain size is under 100 nm, deformation twinning is often rarely observed in HCP metals [50], resulting in poor plasticity. Thus, it is very challenging to enhance the plasticity of nanocrystalline HCP metals.

Here we report on *in situ* micropillar compression studies on mechanical behavior of epitaxial HCP Co (0002) with high-density parallel SFs on basal planes. The *in situ* studies reveal high yield strength, ~1.1 GPa, and prominent work hardening to a flow stress of 2.0 GPa. Post deformation transmission electron microscopy (TEM) analysis shows HCP-to-FCC phase transformation. Molecular dynamics (MD) simulations reveal that the high strength and deformability originate primarily from the phase transformations. This study provides a fresh perspective, that is, phase transformations can be a major deformation mechanism in HCP metals for imparting high strength and plasticity.

2 μm thick Co films were sputter-deposited on hydrofluoric acid etched Si (110) substrates with 100 nm Cu seed layers. The base pressure of the sputter chamber was $4 \times 10^{-6}$ Pa and the deposition rate was ~0.35 nm/s for Co. X-ray diffraction (XRD) experiments were performed by using a Bruker D8 Discover X-ray powder diffractometer at room temperature. Transmission electron microscopy (TEM) experiments were performed on an FEI Talos 200× transmission electron microscope operated at 200 kV. *In situ* micropillar compression tests were performed by using Hysitron PI 88xR PicoIndenter inside an FEI Quanta 3D FEG dual-beam scanning electron microscope (SEM). HCP Co pillars ~1 μm in diameter and ~2 μm in height were fabricated using the same SEM microscope equipped with focused-ion-beam (FIB).

Molecular dynamics simulations were performed on HCP Co nanopillars by using the Large-scale Atomic/Molecular Massively Parallel Simulator (LAMMPS) [51] and the results were visualized using Ovito [52] and DXA [53]. The digital HCP Co pillars were 4 nm in diameter and 8 nm in height and contained stacking faults on the (0002)

* Corresponding author.
*E-mail addresses:* ykulkarni@uh.edu (Y. Kulkarni), xzhang98@purdue.edu (X. Zhang).

https://doi.org/10.1016/j.scriptamat.2019.07.030
1359-6462/

planes. These stacking faults with an average spacing of 1.6 nm were introduced by applying rigid body motion on the (0002) planes along the $<10\bar{1}0>$ direction. Specifically, the layers were held fixed and one rigid block was moved relatively to the other on the (0002) planes in the $<10\bar{1}0>$ direction. Then the entire sample was allowed to relax. First, the pillar was equilibrated at 0 K using the conjugate gradient energy minimization. Subsequently, the sample was equilibrated at 300 K under the NVT ensemble with a Nose-Hoover thermostat. Finally, compression was applied for 160 ps at a strain rate of $6.25 \times 10^8\ s^{-1}$. The Co—Co atomic interactions were described by the embedded-atom method (EAM) potential developed by Zhou et al [54].

XRD pattern in Fig. 1a reveals the epitaxial growth of HCP Co (0002) on Si (110) with 100 nm Cu (111) seed layer. Cross-section TEM micrograph in Fig. 1b shows that the epitaxial HCP Co has a columnar grain size of ~ 50 nm with high-density SFs on basal planes. The inserted selected area diffraction (SAD) pattern also proves the epitaxial growth of HCP Co. Fig. 1c shows the HCP Co has an average SF spacing of ~ 9 nm. The high resolution TEM (HRTEM) micrograph in Fig. 1d shows the SFs in HCP Co, which have FCC stacking.

Mechanical behavior of epitaxial HCP Co (0002) was studied by *in situ* SEM pillar compression testing. Fig. 2a shows the true stress-strain curves. Pillars yield at ~1.2 GPa and show a prominent work hardening capability to a peak stress of ~ 2 GPa. The work hardening exponent is calculated as $n = \sim 0.55$. Fig. 2b-e show SEM snapshots of HCP Co pillar (with respect to the red curve) during compression (see Supplementary Video 1 for details). The HCP Co pillar experiences a uniform deformation without forming any shear bands or cracks up to 20% strain, an indication of prominent plasticity (see Supplementary Fig. S1 for reproducibility check).

Fig. 3 shows TEM micrographs of the deformed HCP Co pillar. Fig. 3a confirms that no shear bands or cracks formed during deformation. There is deformation induced dilation near the pillar top. SAD in Fig. 3a reveals two sets of diffraction patterns, associated with HCP (red lines) and FCC (blue lines) Co, respectively. Higher magnification TEM micrographs in Fig. 3b show multiple sets of inclined SFs. HRTEM micrographs in Fig. 3c-d show the phase boundaries between FCC and HCP Co as decorated by white dashed lines. In FCC Co, the high-density inclined SFs are along (111) planes as determined by the inserted FFTs. Note that the (0002) planes in HCP Co are nearly parallel to the (111) planes in FCC Co (Fig. 3c). The FCC Co phase shown in Fig. 3d is distorted due to plastic deformation.

Deformation modes in HCP metals have been extensively studied. At room temperature, dislocation glide and deformation twinning are two principal deformation mechanisms in HCP metals. For dislocation glide, $<\mathbf{a}>$ type dislocation $[11\bar{2}0]$ gliding on basal or prismatic plane is one of the most common slip systems in HCP metals [55]. However, in this study, the epitaxial HCP Co has (0002) out-of-plane texture, which means the Schmid factors for $<\mathbf{a}>$ type dislocations on both basal and prismatic planes would be very small (close to 0) neither the basal nor the prismatic slip would be the prominent deformation mechanism. Another major dislocation, $<\mathbf{c}+\mathbf{a}>$ type dislocation with Burgers vector of $[11\bar{2}\bar{3}]$, can glide on pyramidal planes and accommodate plastic strain along the **c** direction [55,56]. However, the pyramidal slip of $<\mathbf{c}+\mathbf{a}>$ type of dislocations is largely prohibited by high-density SFs on basal plane [42].

Deformation twinning is another fundamental deformation mechanism in HCP metals due to their limited slip systems [45–49]. However, deformation twinning is largely absent in the TEM micrographs of the deformed HCP Co pillar. Prior studies show that when grain size is <100 nm, deformation twinning may be easier to operate in FCC metals [50,57–59], but becomes much more difficult in HCP metals, except under severe plastic deformation [60] or by adding an alloying element [61]. Since the grain size of HCP Co in this study is ~ 50 nm, deformation twinning is also suppressed during deformation.

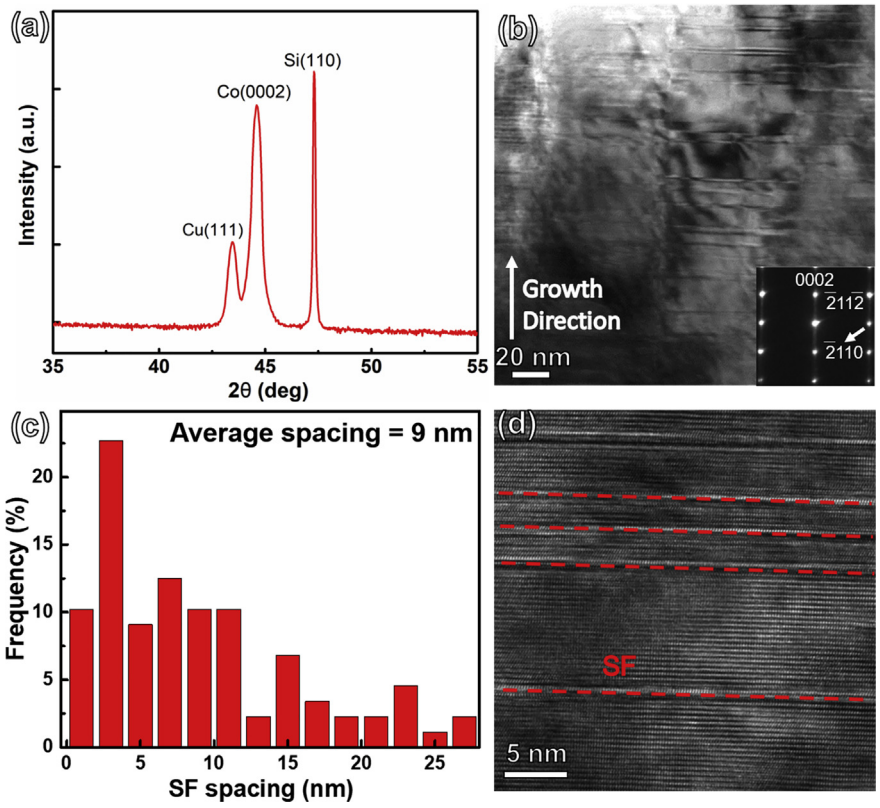


**Fig. 1.** (a). XRD profile showing the epitaxial growth of HCP Co with (0002) orientation on Cu (111) seed layer on Si (110) substrate. (b) Cross-section TEM micrograph showing high-density parallel stacking faults (SFs) on (0002) planes. (c) The SFs have an average spacing of 9 nm. (d) High-resolution TEM (HRTEM) micrograph showing SFs on basal plane of HCP Co.

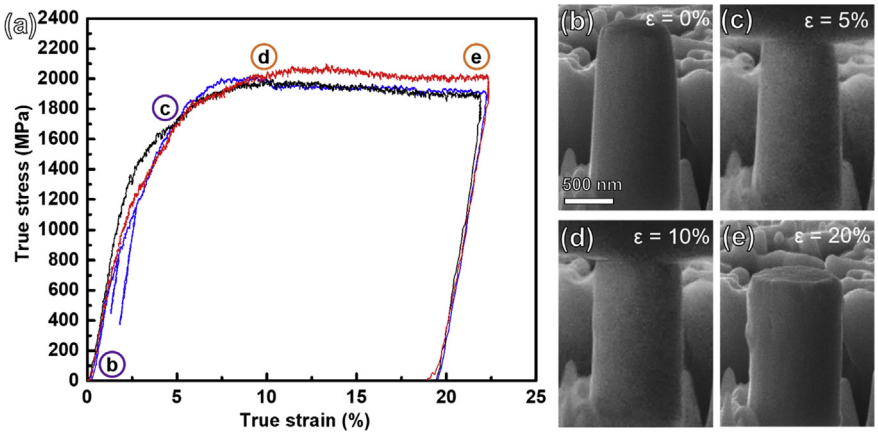


**Fig. 2.** *In situ* micropillar compression tests on HCP Co at a constant strain rate of $5 \times 10^{-3}$/s. (a) True stress-strain curves show HCP Co has a yield strength of ~1.1 GPa with prominent work hardening and compressive plasticity. (b-e) SEM snapshots of an HCP Co pillar showing uniform deformation during compression. No cracks were observed. (See supplementary video 1 for more details).

If the classical dislocation glide and deformation twinning mechanisms are both prohibited in HCP Co with high-density SFs, then how do we explain the deformation mechanisms and work hardening capability observed in the current study? Post compression TEM micrographs (Fig. 3) show the coexistence of both the HCP and the FCC phase in the deformed pillar. As FCC Co was not observed in the as-deposited

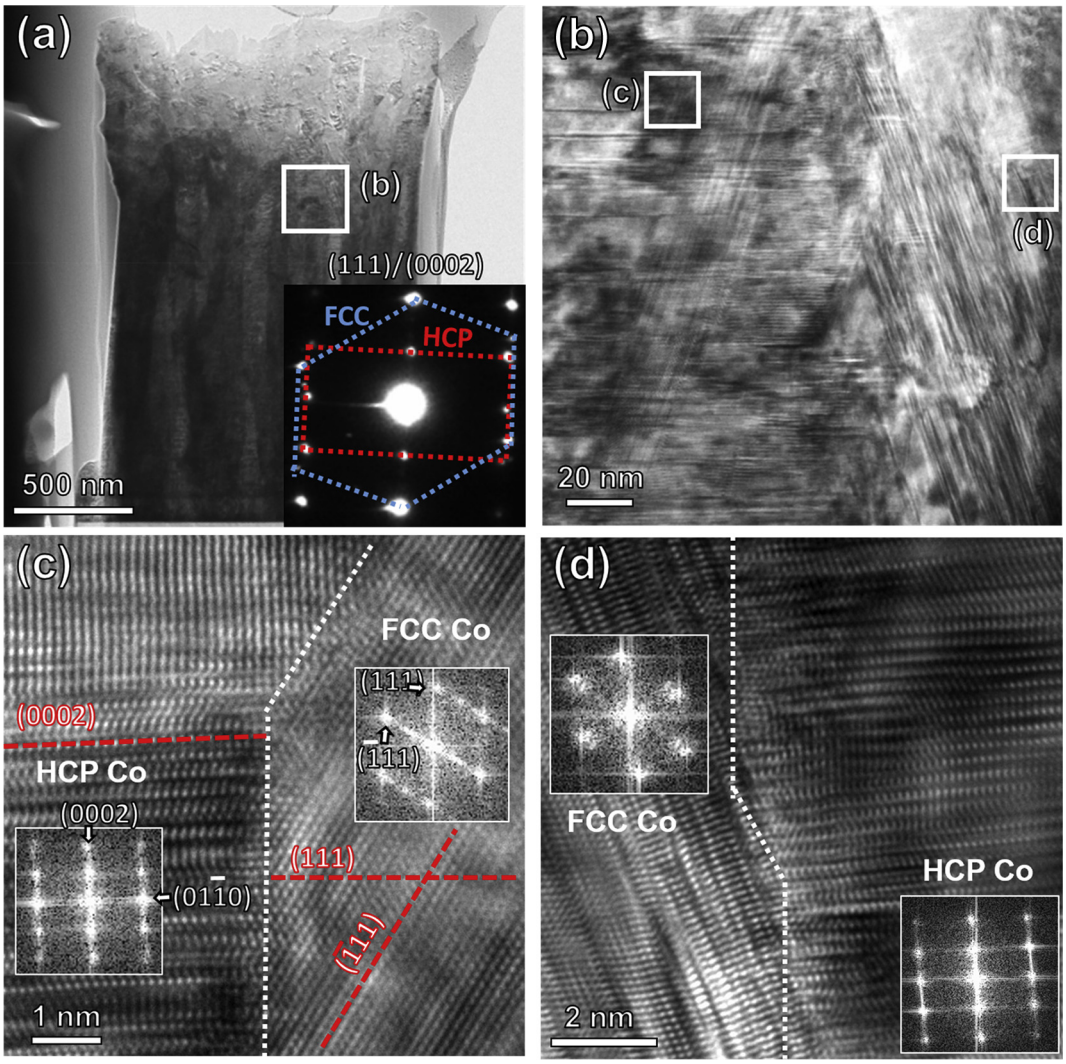


**Fig. 3.** Cross-section TEM micrographs of a HCP Co pillar deformed to ~ 20% true strain. (a) A TEM micrograph at low magnification confirms that there are no shear bands or cracks formed during compression. (b) A higher magnification TEM micrograph of the box (in a) shows inclined SFs (c, d) HRTEM micrographs of the boxes in b show the coexistence of FCC and HCP Co as confirmed by the inserted fast Fourier transform of each region. High-density inclined SFs on the (111) planes were observed in FCC Co.

Co, the FCC phase should have been formed during deformation, which may be triggered by high local stresses [62–64]. TEM micrographs (Fig. 3c-d) show that FCC Co is forms on two sets of inclined (111) planes relative to the horizontal HCP (0002) basal planes. Furthermore high-density inclined SFs along (111) planes in FCC Co are also observed (Fig. 3b) due to the migration of Shockley partial dislocations along the inclined (111) planes. Thus, phase transformation and partial dislocation activity in FCC Co phase may contribute to the significant plasticity during compression of HCP Co.

MD simulations were performed on HCP Co with SFs on basal planes to investigate the atomistic deformation mechanisms and detailed phase transformation process during nanopillar compression. Supplementary Video 2 shows the atomistic view of the compression induced phase transformation process. The stress-strain curve shows a high yield strength of ~12 GPa followed by sharp stress reduction to ~1.8 GPa after yielding (Fig. 4a). Prior to yielding, at about 4% strain, two Shockley partials (green lines) are nucleated at the intersection of the horizontal SFs and the pillar surface (Fig. 4c). With increasing stress, the Shockley partials start to glide along the SF planes resulting in defaulting. Consequently, this partial annihilation of the pre-existing SFs creates space for the FCC Co phase to nucleate and propagate. We have visualized the evolution of the microstructure using the local Von Mises shear strain (Supplementary Fig. S2), which highlights the concentration of local large shear strains around the areas of HCP-to-FCC phase transformation. Fig. 4d shows that, after a patch of FCC Co is formed, Shockley partials nucleate from the interface between the HCP and FCC phases and glide on FCC (111) planes forming SFs in the FCC phase, leading to plastic yielding accompanied with a major stress drop (Fig. 4e). Stair rod dislocations with Burgers vector of 1/6 [110] (red lines) also form at the interception of the inclined SFs by the pre-existing horizontal SFs, which prevent the propagation of partial dislocations and may contribute to work hardening. See Supplementary Video 3 for a view of the dislocations generated during deformation and phase transformation. Crystallographic orientation relationship between HCP and FCC Co revealed by MD simulations is in good agreement with the HRTEM analyses (Fig. 3c-d). It is worth mentioning that Burgers reported a HCP-to-FCC phase transformation mechanism in Zr that is to some extent similar to what MD simulations show in the present study [65]. Another MD simulation of compression of HCP Co without basal plane SFs was also performed. MD simulations show that basal slip and prismatic slip dominate the plastic deformation (Supplementary Fig. S3). These observations indicate that SFs are critical in inhibiting dislocation glide in HCP Co and thus SFs can strengthen the materials.

We report an intriguing deformation mechanism in HCP Co dominated by phase transformation. Epitaxial HCP Co thin films with high

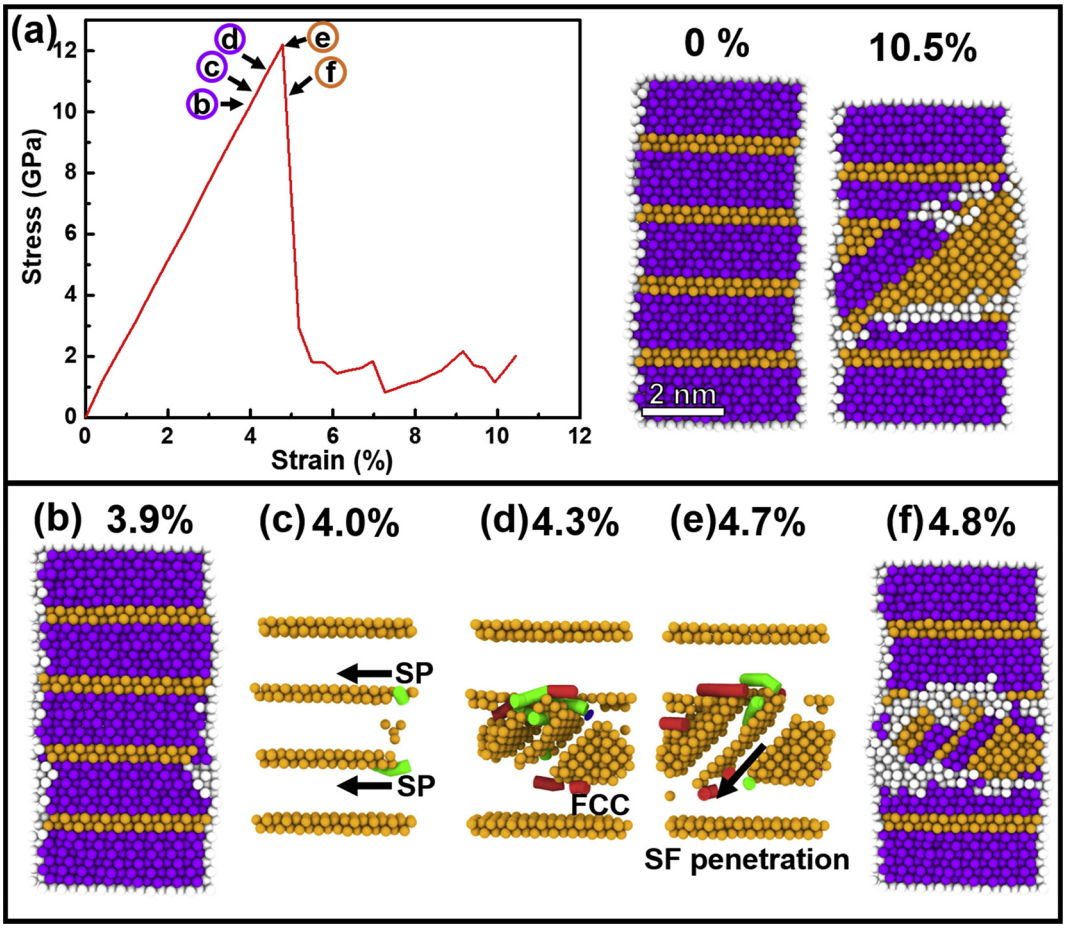


**Fig. 4.** MD simulations of compression tests of HCP Co pillar with parallel SFs. Atoms are in common neighbor color coding, where orange, purple and white denote FCC, HCP and unidentified structures, respectively. Green lines represent Shockley partial dislocations and red lines represent other dislocations including stair rod dislocations. (a) Left panel: The stress-strain curve shows a high yield strength of ~12 GPa followed by sharp stress reduction to ~1.8 GPa after yielding. Right panel: Microstructure of HCP Co pillar before and after compression (at 9.8% strain) revealing. HCP-to-FCC phase transformation occurs. (b) The HCP Co pillar deforms elastically to a strain of ~3.9%. (c) When $\varepsilon = 4.0\%$, Shockley partials nucleated on SF planes. (d) When $\varepsilon = 4.3\%$, the Shockley partials glide along SF planes, causing defaulting of the pre-existing SFs in the HCP phase and the formation of FCC Co on the inclined planes. (e) When $\varepsilon = 4.7\%$, inclined SFs form in FCC Co and penetrate through the parallel SFs where stress drop occurs. (f) When $\varepsilon = 4.8\%$, the population of inclined SFs on (111) plane is increased while some of the horizontal SFs are removed. See supplementary videos 2 and 3 for details. (For interpretation of the references to color in this figure legend, the reader is referred to the web version of this article.)

density SFs exhibit simultaneous high strength and plasticity as revealed by *in situ* SEM compression tests. Post deformation TEM analysis shows the formation of an FCC Co phase during compression. MD simulations elucidate that the HCP-to-FCC phase transformation arises from partial dislocations gliding along the pre-existing SFs parallel to the basal plane during compression. The subsequent generation of inclined SFs on (111) planes in FCC Co plays a key role in accommodating plasticity. Our study provides new perspective for designing high-strength deformable HCP metals by introducing high-density SFs.

Supplementary data to this article can be found online at https://doi.org/10.1016/j.scriptamat.2019.07.030.

## Acknowledgements

RS and XZ acknowledge the financial support by NSF-DMR 1642759. DN and YK acknowledge the financial support by NSF-DMR 1508484. QL is supported by DOE-BES under grant No. DE-SC0016337. H. Wang acknowledges the support from the U.S. Office of Naval Research (N00014-16-1-2778). Access to the Life Sciences Microscopy Center and Materials Science Microscopy Center at Purdue University are also acknowledged. The support from the Core facility for Advanced Computing and Data Science at the University of Houston is also acknowledged. We also acknowledge access to microscopy facilities at DOE Center for Integrated Nanotechnologies.

## References

[1] F. Huang, M.T. Kief, G.J. Mankey, R.F. Willis, Phys. Rev. B 49 (6) (1994) 3962–3971.
[2] R. Naik, C. Kota, J.S. Payson, G.L. Dunifer, Phys. Rev. B 48 (2) (1993) 1008–1013.
[3] P.F. Carcia, A.D. Meinhaldt, A. Suna, Appl. Phys. Lett. 47 (2) (1985) 178–180.
[4] A. Chiba, K. Kumagai, N. Nomura, S. Miyakawa, Acta Mater. 55 (4) (2007) 1309–1318.
[5] M. Srivastava, V. Ezhil Selvi, V.K. William Grips, K.S. Rajam, Surf. Coat. Technol. 201 (6) (2006) 3051–3060.
[6] W. Betteridge, Prog. Mater. Sci. 24 (1980) 51–142.
[7] L. Lu, Y. Shen, X. Chen, L. Qian, K. Lu, Science 304 (5669) (2004) 422–426.
[8] X. Zhang, A. Misra, H. Wang, A.L. Lima, M.F. Hundley, R.G. Hoagland, J. Appl. Phys. 97 (9) (2005).
[9] X. Zhang, H. Wang, X.H. Chen, L. Lu, K. Lu, R.G. Hoagland, Appl. Phys. Lett. 88 (17) (2006).
[10] X.H. Chen, L. Lu, Scr. Mater. 57 (2) (2007) 133–136.
[11] B. Li, B.Y. Cao, K.T. Ramesh, E. Ma, Acta Mater. 57 (15) (2009) 4500–4507.
[12] O. Anderoglu, A. Misra, J. Wang, R.G. Hoagland, J.P. Hirth, X. Zhang, Int. J. Plast. 26 (6) (2010) 875–886.
[13] X. Li, Y. Wei, L. Lu, K. Lu, H. Gao, Nature 464 (7290) (2010) 877–880.
[14] N. Li, J. Wang, J.Y. Huang, A. Misra, X. Zhang, Scr. Mater. 64 (2) (2011) 149–152.
[15] D. Bufford, H. Wang, X. Zhang, Acta Mater. 59 (1) (2011) 93–101.
[16] A.M. Hodge, T.A. Furnish, A.A. Navid, T.W. Barbee Jr., Scr. Mater. 65 (11) (2011) 1006–1009.
[17] N. Li, J. Wang, A. Misra, X. Zhang, J.Y. Huang, J.P. Hirth, Acta Mater. 59 (15) (2011) 5989–5996.
[18] N. Li, J. Wang, X. Zhang, A. Misra, Jom 63 (9) (2011) 62–U62.
[19] D. Bufford, Z. Bi, Q.X. Jia, H. Wang, Appl. Phys. Lett. 101 (22) (2012).
[20] D. Bufford, H. Wang, X. Zhang, J. Mater. Res. 28 (13) (2013) 1729–1739.
[21] D. Bufford, Y. Liu, Y. Zhu, Z. Bi, Q.X. Jia, H. Wang, X. Zhang, Mater. Res. Lett. 1 (1) (2013) 51–60.
[22] D. Bufford, Y. Liu, J. Wang, H. Wang, X. Zhang, Nat. Commun. 5 (2014) 4864.
[23] Y. Liu, J. Jian, Y. Chen, H. Wang, X. Zhang, Appl. Phys. Lett. 104 (23) (2014) 231910.
[24] J. Li, Y. Chen, S. Xue, H. Wang, X. Zhang, Acta Mater. 114 (2016) 154–163.
[25] M. Ardeljan, I.J. Beyerlein, M. Knezevic, Int. J. Plast. 99 (2017) 81–101.
[26] S. Zheng, I.J. Beyerlein, J.S. Carpenter, K. Kang, J. Wang, W. Han, N.A. Mara, 4 (2013), 1696.
[27] F. Sansoz, K. Lu, T. Zhu, A. Misra, MRS Bull. 41 (4) (2016) 292–297.
[28] Z. Zeng, X. Li, L. Lu, T. Zhu, Acta Mater. 98 (2015) 313–317.
[29] A. Kobler, T. Beuth, T. Klöffel, R. Prang, M. Moosmann, T. Scherer, S. Walheim, H. Hahn, C. Kübel, B. Meyer, T. Schimmel, E. Bitzek, Acta Materialia 92(Supplement C) (2015) 299–308.
[30] R. Su, D. Neffati, S. Xue, Q. Li, Z. Fan, Y. Liu, H. Wang, Y. Kulkarni, X. Zhang, Mater. Sci. Eng. A 736 (2018) 12–21.
[31] Y.F. Zhang, S. Xue, Q. Li, C. Fan, R. Su, J. Ding, H. Wang, H. Wang, X. Zhang, Scr. Mater. 148 (2018) 5–9.
[32] S. Xue, W. Kuo, Q. Li, Z. Fan, J. Ding, R. Su, H. Wang, X. Zhang, Acta Mater. 144 (2018) 226–234.
[33] R. Yuan, I.J. Beyerlein, C. Zhou, Acta Mater. 110 (2016) 8–18.
[34] A. Sedlmayr, E. Bitzek, D.S. Gianola, G. Richter, R. Mönig, O. Kraft, Acta Mater. 60 (9) (2012) 3985–3993.
[35] A.M. Hodge, Y.M. Wang, T.W. Barbee, Scr. Mater. 59 (2) (2008) 163–166.
[36] Y. Kulkarni, R.J. Asaro, Acta Mater. 57 (16) (2009) 4835–4844.
[37] Y.M. Wang, F. Sansoz, T. LaGrange, R.T. Ott, J. Marian, T.W. Barbee Jr., A.V. Hamza, Nat. Mater. 12 (8) (2013) 697–702.
[38] J. Wang, O. Anderoglu, J.P. Hirth, A. Misra, Appl. Phys. Lett. 95 (2) (2009).
[39] Z.X. Wu, Y.W. Zhang, D.J. Srolovitz, Acta Mater. 57 (15) (2009) 4508–4518.
[40] N. Lu, K. Du, L. Lu, J. Appl. Phys. 115 (2) (2014).
[41] L. Lu, X. Chen, X. Huang, K. Lu, Science 323 (5914) (2009) 607–610.
[42] W.W. Jian, G.M. Cheng, W.Z. Xu, H. Yuan, M.H. Tsai, Q.D. Wang, C.C. Koch, Y.T. Zhu, S. N. Mathaudhu, Mater. Res. Lett. 1 (2) (2013) 61–66.
[43] W.F.J.O.U.P. Hosford, „ (1993) 248.
[44] R. Hill, The mathematical theory of plasticity, Oxford university press1998.
[45] Y. Li, Y. Chen, J.C. Walmsley, R. Mathinsen, S. Dumoulin, H.J.J.S.M. Roven, 62(7) (2010) 443–446.
[46] G.G. Yapici, I. Karaman, Z.-P. Luo, Acta Mater. 54 (14) (2006) 3755–3771.
[47] I. Kim, J. Kim, D.H. Shin, X.Z. Liao, Y.T. Zhu, Scr. Mater. 48 (6) (2003) 813–817.
[48] Q. Yu, Z.-W. Shan, J. Li, X. Huang, L. Xiao, J. Sun, E. Ma, Nature 463 (7279) (2010) 335–338.
[49] Y.B. Wang, M. Louie, Y. Cao, X.Z. Liao, H.J. Li, S.P. Ringer, Y.T. Zhu, Scr. Mater. 62 (4) (2010) 214–217.
[50] Y.T. Zhu, X.Z. Liao, X.L. Wu, Prog. Mater. Sci. 57 (1) (2012) 1–62.
[51] S. Plimpton, J. Comput. Phys. 117 (1) (1995) 1–19.
[52] A. Stukowski, Mater. Sci. Eng. 18 (1) (2010), 015012.
[53] A. Stukowski, V.V. Bulatov, A. Arsenlis, Modelling and Simulation in Materials Science and Engineering 20(8) (2012) 085007.
[54] X.W. Zhou, R.A. Johnson, H.N.G. Wadley, Phys. Rev. B 69 (14) (2004) 144113.
[55] M.J.M.T.A. Yoo, 12(3) (1981) 409–418.
[56] Z. Wu, W.A. Curtin, Proceedings of the National Academy of Sciences of the United States of America 113(40) (2016) 11137–11142.
[57] V. Yamakov, D. Wolf, S.R. Phillpot, H. Gleiter, Acta Mater. 50 (20) (2002) 5005–5020.
[58] M.W. Chen, E. Ma, K.J. Hemker, H.W. Sheng, Y.M. Wang, X.M. Cheng, Science 300 (5623) (2003) 1275–1277.
[59] X.Z. Liao, Y.H. Zhao, S.G. Srinivasan, Y.T. Zhu, R.Z. Valiev, D.V. Gunderov, Appl. Phys. Lett. 84 (4) (2004) 592–594.
[60] L. Zhang, Y. Han, Mater. Sci. Eng. A 523 (1) (2009) 130–133.
[61] X.L. Wu, K.M. Youssef, C.C. Koch, S.N. Mathaudhu, L.J. Kecskés, Y.T. Zhu, Scr. Mater. 64 (3) (2011) 213–216.
[62] J.Y. Huang, Y.K. Wu, H.Q. Ye, Appl. Phys. Lett. 66 (3) (1995) 308–310.
[63] F. Delogu, Scr. Mater. 58 (2) (2008) 126–129.
[64] J. Sort, N.M. Mateescu, J. Nogués, S. Suriñach, M.D. Baró, J. Metast. Nanocryst. Mater. 12 (2002) 126–133.
[65] W.G. Burgers, Physica 1 (7) (1934) 561–586.